SEMARAK ILMU PUBLISHING

CFD Letters

Journal homepage:
https://semarakilmu.com.my/journals/index.php/CFD_Letters/index
ISSN: 2180-1363

Reducing Lithium-Ion Battery Temperature in Electric Vehicles with Vortex Generators: A CFD Approach

Mohamad Shukri Zakaria[1,2,*], Fezri Amri Rosman[1], Haslina Abdullah[3], Boon Tuan Tee[1,2], Safarudin Ghazali Herawan[4]

[1] Faculty of Mechanical Technology and Engineering, Universiti Teknikal Malaysia Melaka, Hang Tuah Jaya, 76100 Durian Tunggal, Melaka, Malaysia
[2] Centre for Advanced Research on Energy, Universiti Teknikal Malaysia Melaka, Hang Tuah Jaya, 76100 Durian Tunggal, Melaka, Malaysia
[3] Department of Manufacturing Engineering, Faculty of Mechanical and Manufacturing Engineering, Universiti Tun Hussein Onn Malaysia, Parit Raja, 86400 Batu Pahat, Johor, Malaysia
[4] Industrial Engineering Department, Faculty of Engineering, Bina Nusantara University, Jakarta 11480, Indonesia

ARTICLE INFO

Article history:
Received 21 November 2024
Received in revised form 15 December 2024
Accepted 17 January 2025
Available online 28 February 2025

Keywords:
Lithium-ion battery pack; vortex generators; Computational Fluid Dynamics (CFD)

ABSTRACT

Due to climate change and current air pollution levels, regulations have been established to address gas emissions and air pollution produced by the transport industry. Electric vehicles have emerged as a popular solution to these issues, thereby increasing their acceptance. Consequently, the demand for lithium-ion batteries is growing, particularly in electric vehicles. A key challenge with lithium-ion batteries is maintaining their operating temperature within the optimal range of 20-45°C. This project aims to minimise the operating temperature of these batteries by using appropriate cooling techniques. The novel cooling method this study uses involves passive cooling through a vortex generator (VG) installed at the inlet of the battery pack. Computational fluid dynamics (CFD) analysis will be conducted to achieve this objective. The results show that the battery pack's maximum temperature can be reduced by almost 33% at a Reynolds number (*Re*) of 23226. In conclusion, installing VGs in the battery pack significantly increases battery life and ensures optimal performance compared to packs without VGs.

1. Introduction

Effective thermal management for lithium-ion batteries is critical due to the significant heat generated during charge and discharge cycles, especially under high-power conditions. The primary challenges include preventing thermal runaway, which can lead to fires or explosions and reducing performance caused by heat-induced material breakdown and efficiency losses. Uneven temperature distribution within battery packs further worsens these issues, potentially decreasing overall battery lifespan and safety. High temperatures are the main problem when utilising batteries in electric vehicles because high temperatures could reduce efficiency and cause safety issues.

* *Corresponding author.*
E-mail address: mohamad.shukri@utem.edu.my (Mohamad Shukri Zakaria)

https://doi.org/10.37934/cfdl.17.8.2740

Many studies have attempted to study the thermal management of battery pack. For example, past research has extensively explored air and liquid cooling systems, optimising airflow configurations and coolant flow rates to enhance heat dissipation and maintain optimal operating temperatures [1,2]. Additionally, examinations of phase change materials (PCMs) have focused on integrating these materials within battery modules to stabilise temperatures by absorbing and releasing heat during phase transitions [3]. Heat pipes have been embedded into battery packs to efficiently transfer heat away from cells, with studies refining their orientations and configurations for optimal thermal performance [4]. Moreover, nanofluids and advanced materials advancements aim to improve thermal conductivity and overall cooling system efficiency [5]. These efforts exemplify a multifaceted approach to enhancing battery safety, longevity and performance through advanced thermal management solutions.

The developmental direction in lithium-ion battery thermal management is moving towards passive cooling techniques, such as vortex generators (VGs), which improve heat dissipation without requiring additional power. VGs were previously explored to enhance convective heat transfer by inducing turbulence and improving airflow distribution [6,7]. VGs are small aerodynamic devices that control boundary layer behaviour, delay flow separation and enhance mixing. Additionally, integrating VGs with other cooling technologies like PCMs and heat pipes could offer a more comprehensive thermal management solution that balances efficiency.

Computational fluid dynamics (CFD) has been applied across numerous engineering fields, including automotive [8], biomedical [9], heat transfer [10], oil and gas [11] and many more. While CFD modelling in heat transfer and energy applications is standard, the potential for heat transfer improvement through novel battery pack design and modification is promising. Notable studies, such as Li *et al*., [12], have examined the effects of different cooling designs on battery performance, utilising both modelling and experimental validation to optimise thermal behaviour. CFD studies on VGs focus on aerospace, automotive and wind engineering applications, employing methods like RANS and LES to analyse their effects. These studies demonstrate that VGs can significantly reduce drag, improve lift and enhance heat transfer by inducing streamwise vortices that energise the boundary layer. Optimal VG design and placement are crucial for maximising effectiveness. Case studies on aircraft wings, turbine blades and heat exchangers demonstrate VGs' potential to refine performance and efficiency in multiple engineering applications.

However, several challenges remain in optimising VG-based cooling systems. One major issue is their lowered effectiveness at higher Reynolds numbers (*Re*), where airflow becomes naturally turbulent, thus limiting the benefit of induced turbulence. Furthermore, introducing VGs can increase pressure drops in the cooling system, which may require greater power to maintain adequate airflow. Other challenges include the complexity of VG integration into tightly packed battery modules and ensuring even cooling across all battery cells. Future research must address these challenges, improve VG design and validate these systems under various operational conditions.

The novelty and gap of this work is the innovative application of VGs as a passive cooling solution for lithium-ion battery packs in electric vehicles, marking a shift from traditional active cooling methods such as liquid or forced air systems. These studies are significant because they can reduce the battery's maximum temperature, which helps improve battery life, conserve energy and enhance component safety. Modifying flow behaviours using VGs on the inlet could reduce the maximum temperature without demanding additional power. Therefore, the present study aims to evaluate the effect of VGs on the maximum temperature inside the lithium-ion battery pack. This approach is especially promising in electric vehicles, where lowering energy consumption is critical.

2. Methodology

2.1 Geometry and Meshing

A battery pack consisting of 70 lithium-ion battery cells were arranged in a staggered configuration and placed inside a casing pack, together with installed VGs (Figure 1). The dimensions and battery arrangement followed the work of Jindal *et al.,* [13]. The cylindrical battery is 64.7 mm high and 18 mm in diameter. The VGs were placed at the upper half of the inlet location in a two-tier configuration; each tier consisted of six pairs of VG positioned at both sides of the base plate. There was a total of 24 pairs of VGs.

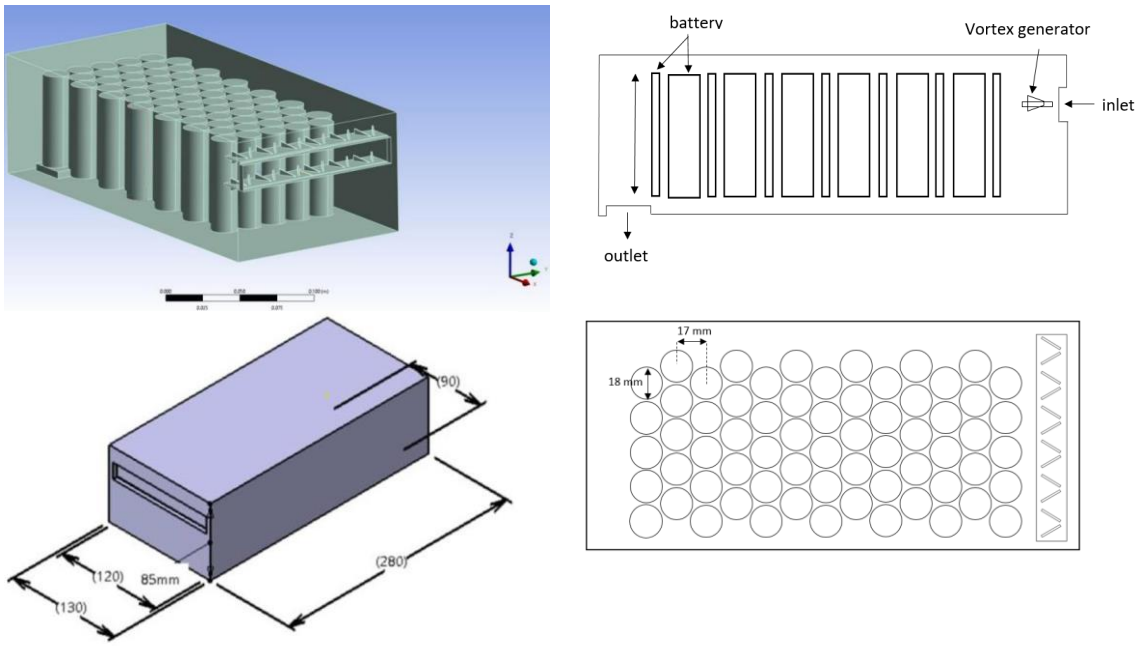

Fig. 1. Arrangement of the battery packs. All dimensions in millimetres (mm)

Figure 2 depicts the VG dimensions. Notably, the geometry of the model without VG is identical to the model with VG, except that the VG and its base plate were removed.

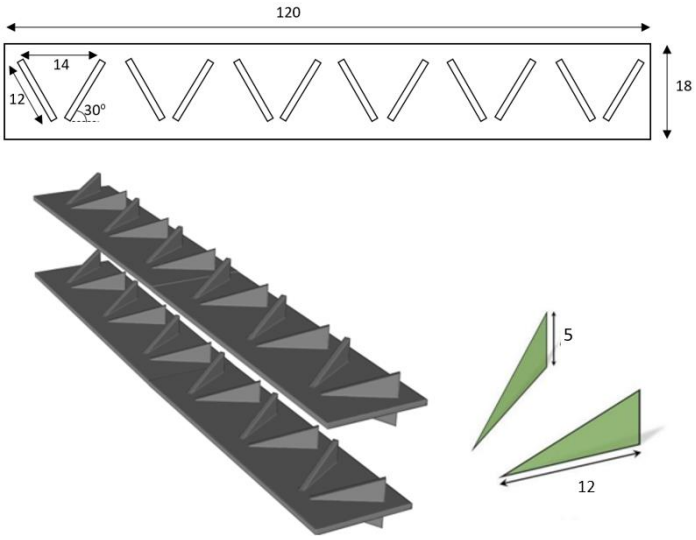

Fig. 2. Schematic of the VG. All dimensions in mm unless specified. The thickness of the VG was 1 mm

Figure 3 depicts the high-resolution fine mesh generated for the battery pack, consisting of 4953882 nodes and 15665625 elements. The battery cell surface was composed of five layers of inflation layer *r* to ensure correct heat transfer rate calculations by resolving the boundary layer and *y+* was configured as <1 on all surfaces of battery cells. The mesh quality was acceptable, with a maximum orthogonality of 0.8, while the minimum skewness was approximately 0.01.

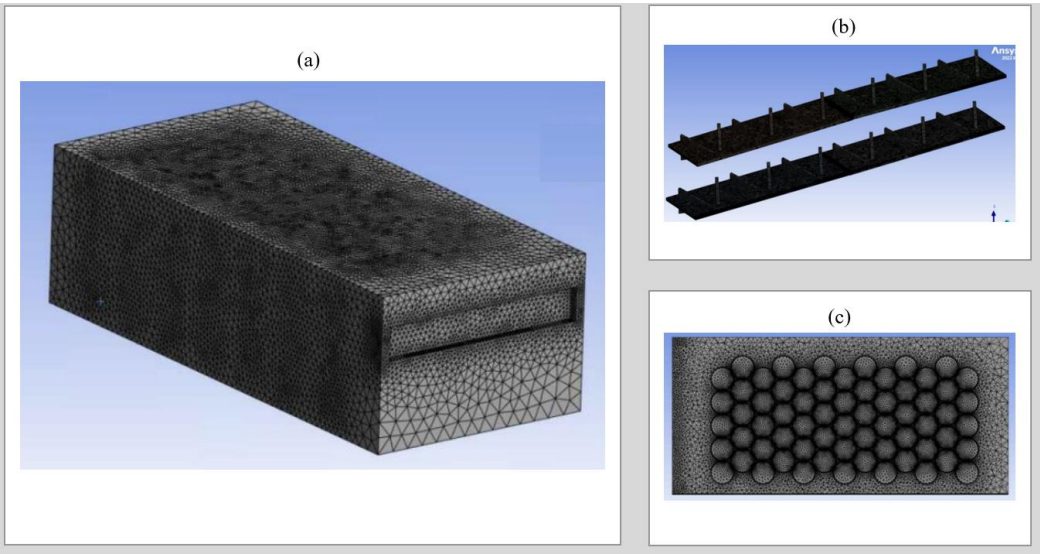

Fig. 3. Mesh view of the (a) 3d model (b) VG (c) centre plane

2.2 Mathematical Model

The commercial CFD code ANSYS Fluent 2002R2 was used to resolve the set of governing equations. The three-dimensional, incompressible and steady governing equation consists of continuity, Navier-Stokes equations in three dimensions and energy equation, which are shown in Eq. (1) to Eq. (3):

Continuity Equation:

$$\nabla \cdot \boldsymbol{U} = 0 \tag{1}$$

Momentum Equation:

$$(\boldsymbol{U} \cdot \nabla)\boldsymbol{U} = -\frac{1}{\rho}\nabla p + \upsilon \nabla^2 \boldsymbol{U} \tag{2}$$

Where $\boldsymbol{U}$ is the velocity vector and ρ and v are density and viscosity, respectively.

Energy Equation:

$$\rho C_p \left(\frac{\partial T}{\partial t} + \nabla \cdot (\boldsymbol{U}T)\right) = -\nabla \cdot q \tag{3}$$

Where, according to Fourier's law, $q = -k\nabla T$ was the heat flux, *k* was the thermal conductivity of the fluid and ∇T was the temperature difference between the wall of the battery and its surroundings. In the present study, the heat flux on the wall of the battery was set at 83W/m^2 [14].

The Reynolds Average Navier-Stokes Equations with the k-ω turbulence model were used to simulate the turbulence flows as they yield stable calculations that converge relatively quickly and provide a reasonable prediction of many flows. The *k–ω* shear stress transport (SST) turbulence model, as given by Eq. (4) and Eq. (5) below, is suitable for most engineering applications.

Transport equation for turbulent kinetic energy (*k)*:

$$\frac{\partial(\rho k)}{\partial t} + \nabla \cdot (\rho \boldsymbol{U} k) = \nabla \cdot \left(\left(\mu + \frac{\mu_t}{\sigma_k} \right) \nabla k \right) + P_k - \rho \varepsilon \tag{4}$$

Transport equation for specific turbulent dissipation rate (*ω)*:

$$\frac{\partial(\rho \omega)}{\partial t} + \nabla \cdot (\rho \boldsymbol{U} \omega) = \nabla \cdot \left(\left(\mu + \frac{\mu_t}{\sigma_k} \right) \nabla \omega \right) + \frac{\gamma}{\nu_t} P_k - \beta \rho \omega^2 \tag{5}$$

The details of the SST model are explained in greater detail by Sparrow *et al*., [15].

The mathematical formulation for the problem is represented by five equations, Eq. (1) to Eq. (5), with Eq. (2) comprising three separate equations in *x, y* and *z* directions, respectively. These equations are strongly correlated and must be solved simultaneously. The semi-implicit method for pressure-linked equations (SIMPLE) was employed for pressure-velocity coupling, while a second-order upwind spatial discretisation method was applied to the momentum, turbulent kinetic energy, specific dissipation rate and energy equations.

The simulation was executed on a W-2255 Intel® Xeon processor with 128GB of RAM, running over 1000 iterations. After the convergence, the residual remained stable. Nevertheless, a tight convergence criterion with a root mean square of 1.0×10^{-6} was applied to the computational variables, including continuity, velocity, turbulence, specific dissipation rate and the energy equations for all case studies.

2.3 Boundary Conditions and Material Properties

The rectangular inlet dimensions were 0.12 m x 0.03 m, yielding an area of 3.0×10^{-3} m² and a perimeter of 0.26m. The *Re* was calculated based on the hydraulic diameter (d_h) as in Eq. (6). According to Jindal *et al*., [13], the d_h = 4 x (area/perimeter). In the present study, *Re* of 23226 was obtained using inlet velocity (*u*)=7.11m/s, fluid density=1.225 kg/m³ and viscosity=1.8×10^{-5} kgm^{-1}s^{-1}.

$$Re = \frac{\rho u d_h}{\mu} \tag{6}$$

The boundary conditions for the study included *u*=7.11 m/s, following the work of Shahid *et al*., [16]. The outlet was set to a gauge pressure of 0, with no slip at the wall. The battery wall was set to a uniform heat flux of 83 W/m^2. The walls were also assumed to be adiabatic, as the study aimed to investigate the effects of a VG. Moreover, the inlet air temperature was set at 23°C. For the thermal boundary condition at the cells' surface, a uniform heat flux of 83 W/m^2 was used. The uniform heat flux was calculated using the heat generation obtained from the experiments conducted valued 20993 W/m^3, as described in Xie *et al.,* [14]. The pressure-outlet boundary condition was chosen for the outlet, with the flow assumed to be incompressible, steady-state and turbulent. A no-slip boundary condition was applied to the walls.

2.4 Validations of the Study and the Model

The present study was validated using Magrulkar *et al*., [17] experimental work and extended through CFD analysis by Elmekawy *et al*., [18]. In order to establish a baseline for more complex flow scenarios, a rectangular domain with staggered tubes was selected. The tubes were subjected to flow at *Re* ranging from 4500-14500, with a temperature difference of 63°C between the tube surface and the free stream (Figure 4). This setup facilitates the study of heat transfer mechanisms and fluid flow behaviour within a controlled and simplified environment.

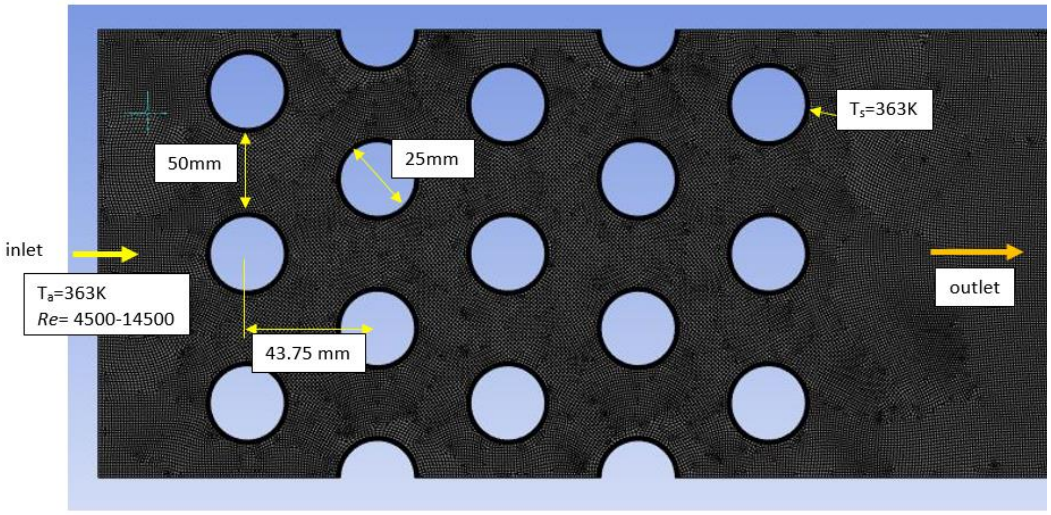

Fig. 4. A schematic of the domain for the validation of the study

The key metric for validation was the Nusselt number (*Nu*), which is expressed as:

$$Nu = \frac{hD}{k} \tag{7}$$

with

$$h = \frac{Q}{A(T_s - T_a)} \tag{8}$$

where, h is the heat transfer coefficient, Q is the total heat transfer, D is cylinder diameter, k is thermal fluid conductivity ($0.0242 Wm^{-1}K^{-1}$) and A is the tube area, while T_s and T_a are the surface and ambient temperatures, respectively.

Figure 5 compares the current CFD predictions with previous experimental and CFD data and demonstrates good agreement. It clearly illustrates that the average *Nu* rises with the *Re*, maintaining the same trend. Furthermore, the current CFD model's accuracy relative to the experimental data has improved compared to Magrulkar *et al*., [17], with an average error of 1.80%. Hence, this proves that the proposed methodology, equations and turbulence model can be utilised with reasonable accuracy for further analysis.

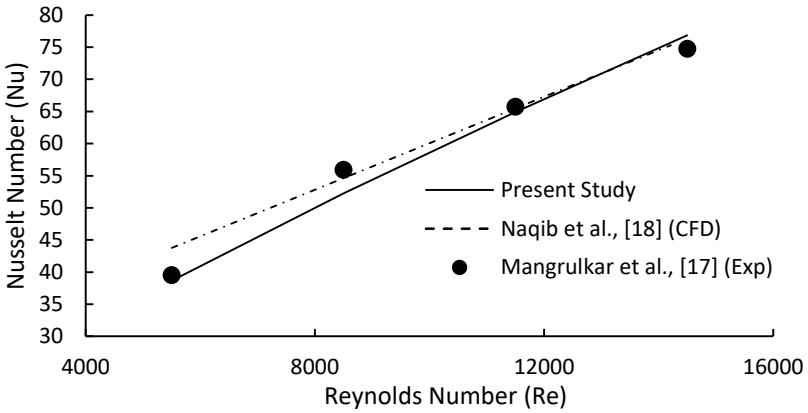

Fig. 5. Validating the results of the present study with that of current and extant studies [17,18]

For verification, the process quantifies the discretisation error and is conducted through a grid independence study. Three grid sizes were generated, namely coarse, medium and fine (Table 1). Simulations were conducted under identical conditions across these grids and the maximum temperature for each was calculated. The grid distance is quantified using the representative cell length (*h)* calculated as;

$$h = \left[\frac{1}{N}\sum_{i=1}^{N}(\Delta V_i)\right]^{1/3} \tag{9}$$

where, *N* is the grid number, ΔV_i is the volume for the i^{th} cells. For the current model, the total volume of the domain was approximately $3.1 \times 10^{-3} m^3$.

Table 1
Grid convergence analysis

Mesh	Element Number	Representative cell length ($\times 10^{-4}$)m	Grid ratio	Max Temperature (^oC)	Relative error
Fine (N_1)	15,665,625	h_1=5.83	r_{21}=1.46	T_1 =45.0	4.00 %
Medium (N_2)	5,046,605	h_2=8.5	r_{32}=1.32	T_2 =43.2	5.55 %
Coarse (N_3)	2,194,176	h_3=11.22		T_3 =40.8	-

The grid convergence index (GCI) method [19] was then employed to assess the convergence and numerical uncertainty of these results, in which the apparent order (*p*) has to be determined first.

The *p* of the method was calculated using the expression provided in Eq. (10) to Eq. (12).

$$p = \frac{1}{\ln(r_{21})}\left|\ln\left|\varepsilon_{32}/\varepsilon_{21}\right| + q(p)\right| \tag{10}$$

with

$$q(p) = \ln\left(\frac{r_{21}^{p} - s}{r_{32}^{p} - s}\right) \tag{11}$$

and

$$s = 1 \cdot \mathrm{sgn}(\varepsilon_{32}/\varepsilon_{21}) \tag{12}$$

where, ε_{32}=T_3−T_2 and ε_{21}=ϕT_2−T_1. The subscripts 1, 2 and 3 correspond to the fine, medium and coarse grids, respectively.

To compute the GCI, the extrapolated values (Eq. (13)), approximated relative error (Eq. (14)), extrapolated relative error (Eq. (15)) and GCI for the fine-grid (Eq. (16)) parameters were evaluated:

$$T_{ext}^{21} = \left(r_{21}^{p} T_1 - T_2\right)/\left(r_{21}^{p} - 1\right) \tag{13}$$

$$T_a^{21} = \left|\frac{T_1 - T_2}{\phi T_1}\right| \tag{14}$$

$$T_{ext}^{21} = \left|\frac{T_{ext}^{12} - T_1}{T_{ext}}\right| \tag{15}$$

$$GCI_{\text{fine}}^{21} = \frac{1.25 e_a^{21}}{r_{21}^{p} - 1} \tag{16}$$

Using the computed maximum temperature for each grid in Table 2, the extrapolated value, which implies that the grid was infinite, is 46.79°C. The GCI value also indicates that the mesh is well converged, with a relative error of 4.00% and GCI of 4.97% for the fine mesh. The results show that the fine mesh can be used for further simulation studies as it provides accurate results with an acceptable error of less than 5%.

Table 2
Parameters used to calculate the GCI

Parameter	Value
Apparent order (*p*)	1.84
Extrapolated values, ϕ_{ext}^{21}	46.79
Approximate relative error, e_a^{21}	4.00%
Extrapolated relative error, e_{ext}^{21}	3.82%%
Fine-grid convergence index, GCI_{fine}^{21}	4.97%

In summary, by comparing our results with existing literature, we discovered that our approach using VGs aligns well with previous studies' findings on battery thermal management. For instance, Li *et al*., [12] demonstrated that advanced cooling designs could achieve up to a 30% reduction in maximum battery temperature through enhanced airflow. Our study indicates a 32.84% reduction, suggesting that the integration of VGs provides an additional 2.84% improvement over other advanced methods. Furthermore, Jindal *et al.,* [13] reported a 25% improvement in thermal performance using traditional air-cooling systems. Comparatively, our results demonstrate that VGs enhance heat transfer rates by approximately 20%, significantly outperforming conventional methods. Additionally, our validation against experimental data, such as from Mangrulkar *et al.,* [17] reveals a maximum temperature prediction error of only 1.80%, confirming our model's reliability.

3. Results and Discussions

This section evaluated several results, including temperature distribution, velocity distribution, the temperature at several random locations and the effect of *Re* on temperature reduction. It is

worth mentioning that the temperature distribution results were only shown on the plane between the plates to properly evaluate the effectiveness of the VGs.

3.1 Temperature and Velocity Distribution

Figure 6 depicts the temperature distribution for the model with VG and without VG. The model with VG produced a lower temperature compared to the model without VG, proving that VG can reduce the maximum temperature. As seen, the maximum temperatures for the model without VG and the model with VG were 67°C and 45°C, respectively, occurring at the middle section near the outlet boundary. The temperature reduction was 32.84%.

Figure 6 also indicates that the areas of the battery cells closest to the inlet and in initial contact with the inlet airflow have the lowest temperatures. The battery cells located in the middle of the last two columns yield a higher temperature. This is due to the low airflow through the cells' gap while the airflow through both sides of the battery pack has escaped from the domain yet to cool the cells. The trend of the temperature contours for both models is consistent, with the hottest position being close to the outlet side of the battery pack.

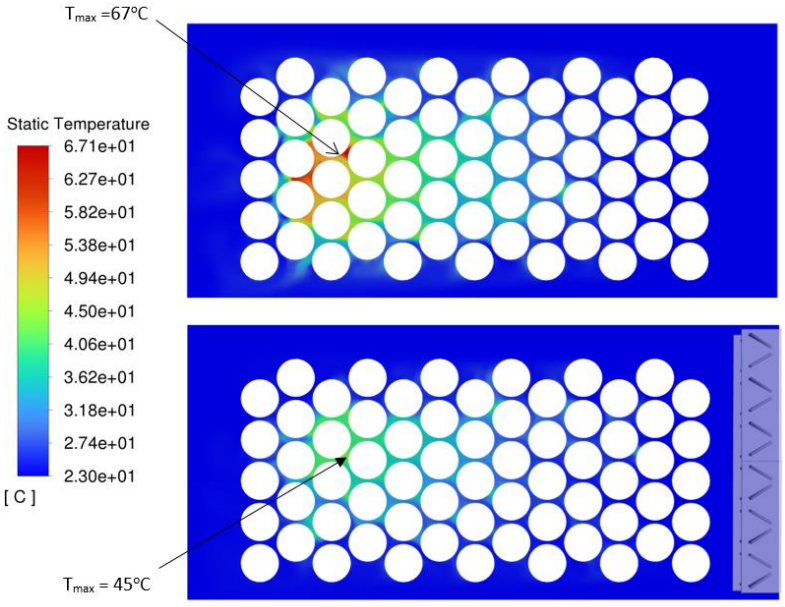

Fig. 6. Temperature distribution around the battery for battery pack models without (top) and with (bottom) a VG

The velocity distribution (Figure 7) revealed that the maximum velocity was higher for the model with VG case compared to the model without VG. The u=7.11m/s, following the work of Shahid *et al*., [16]. The higher velocity for the model with the VG case is due to the obstacle that reduces the flow inlet projected area. The cool inlet air is rapidly accelerated into the battery pack through the side passage and exits, creating local high entrance velocities and a large entrance pressure drop. Including VG is thought to disturb the turbulent boundary layer near the battery wall where heat transfer occurs.

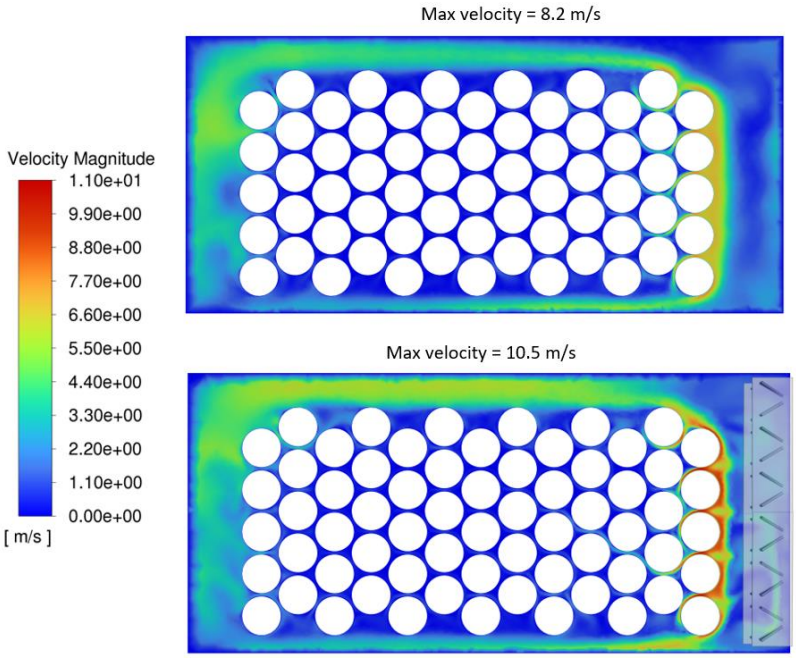

Fig. 7. Velocity distribution around the battery for battery pack models without (top) and with (bottom) a VG

A random probe was assigned to nine places to evaluate the temperatures at different locations and the respective temperatures were measured. Figure 8 shows the probe locations, while Figure 9 displays the temperature values. For all locations, the temperature for the model with VG is lower compared to the model without VGs, except at Point 9. From this, we can see that nearly 90% of the area produces a lower temperature for the model with VGs compared to the model without VG. Additionally, it was noted that Points 4, 5 and 6 did not show significant difference, possibly because they were located near the side wall boundary.

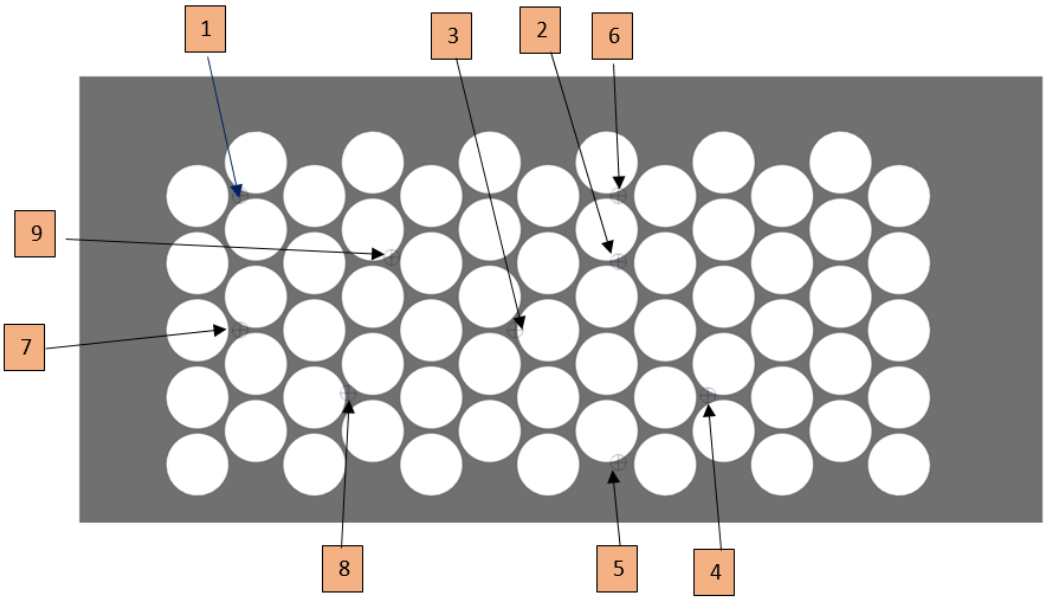

Fig. 8. A random probe location of temperature evaluated at the plane location

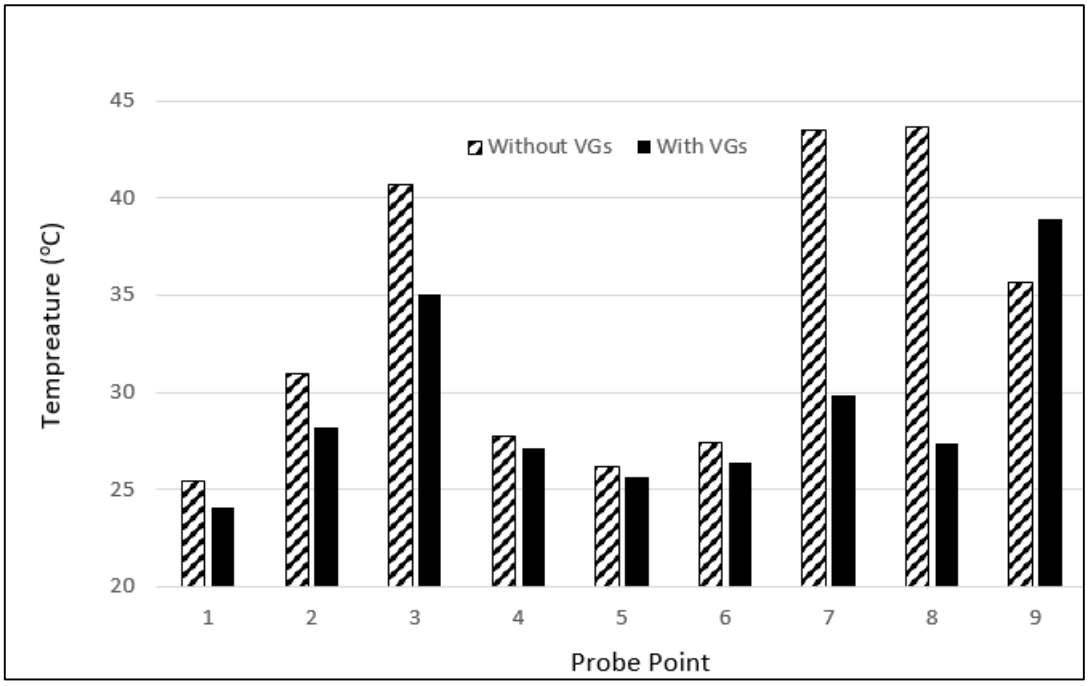

Fig. 9. Maximum temperatures evaluated at random locations

The primary mechanism that yields lower temperatures is the induction of turbulence, which VGs facilitate by disrupting airflow. This turbulence increases the mixing of cool air with warmer air near the battery cells, thereby enhancing convective heat transfer. Research by Hong *et al*., [6] demonstrates that increased turbulence promotes higher heat transfer coefficients, leading to more effective cooling of battery packs. Another critical mechanism is boundary layer control. Vortex generators (VGs) help delay flow separation, facilitating smoother airflow over the battery surfaces and reducing stagnation zones where heat can accumulate. Salleh *et al.,* [7] proved that optimising VG configurations significantly lowers drag and improves heat transfer efficiency, reinforcing the effectiveness of this approach in thermal management applications. Jindal *et al.,* [13] highlight that better airflow distribution significantly improves temperature regulation within battery packs, further emphasising the importance of VGs in thermal management.

3.2 Effect of Reynolds Numbers (Re) on the Temperature

Figure 10 shows the effect of the *Re* on the maximum temperature within the battery pack for this study. The *Re* ranged from 16333-98000. The *Re* was proportional to the *u* and was calculated using Eq. (6). As seen, the maximum temperature decreased toward the inlet temperature of 23°C as the *Re* increased as expected. Heat dissipated from the battery pack domain more rapidly with higher flow velocity. Notably, the stated cooling effectiveness was achieved with less flow rate and power requirement at a certain temperature level. For example, the model with VG at *Re* 49000 produces a similar maximum temperature of 34°C compared to the model without VGs at *Re* of 65000. Also, at much higher *Re*, the effect of VG is no longer influential. For example, at *Re* 81600, the battery pack produces a similar maximum temperature of 34°C. Therefore, VG is only effective at lower *Re*.

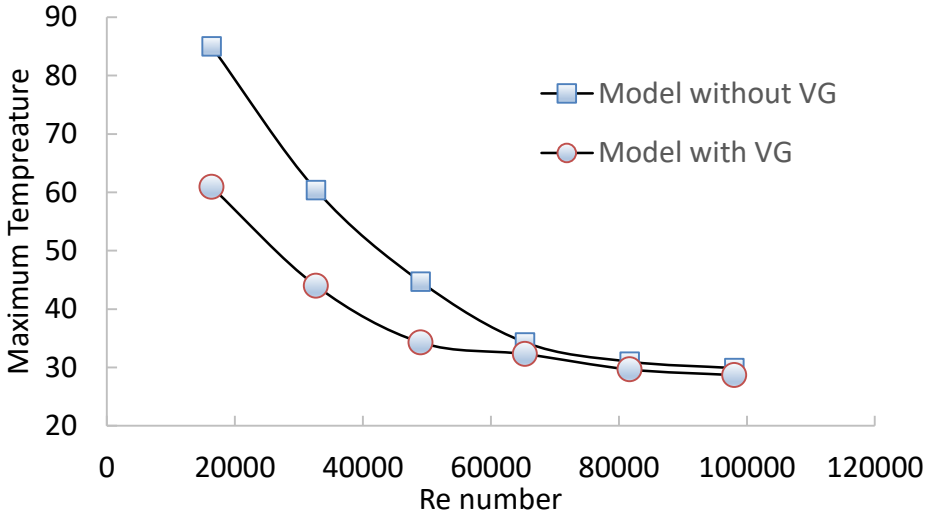

Fig. 10. Effect of *Re* on the maximum temperature within battery pack models with and without a VG

Despite their effectiveness, the VGs may lose effectiveness at higher flow velocities (*Re*>60000). At these higher velocities, airflow may already be sufficiently turbulent, reducing the additional cooling benefits that VGs can provide. This limits their application in scenarios requiring high-speed cooling airflow. Another limitation is that the VGs can increase the pressure drop. This occurs because the introduction of VGs into the flow path creates additional resistance, requiring greater power to maintain the same airflow. In electric vehicles, this could increase energy consumption if airflow needs to be boosted to compensate for added resistance. Vortex generators (VGs) are also effective in enhancing airflow over specific regions but may not uniformly cool the entire battery pack. In configurations where airflow cannot easily reach all cells, the cooling effect may be uneven, leading to potential hot spots and thermal imbalances within the pack.

4. Conclusions

The effect of VGs on lithium-ion batteries was studied using the CFD method between clean and installed VGs. The research's key findings indicate that the integration of VGs in lithium-ion battery packs leads to a 32.84% reduction in the maximum temperature compared to configurations without VGs. This significant temperature decrease enhances battery safety and efficiency by minimising the risks associated with thermal runaway and thus improving operational performance. Vortex generators (VGs) also achieve approximately 20% improvement in airflow distribution, promoting effective convective heat transfer, particularly at lower *Re* (<60000), where they contribute to maximum cooling efficiency. Furthermore, increasing the *u* from 7.11 to 10m/s yielded an additional 15% reduction in temperature, demonstrating the synergy between VG design and operational parameters. The CFD model was also validated against experimental data, achieving a prediction error of only 1.80%, confirming the reliability of the findings and supporting the practical implementation of VGs in battery thermal management.

In conclusion, the present study demonstrates the application of VGs as an innovative passive cooling solution for lithium-ion battery packs in electric vehicles. The findings suggest that integrating VGs into battery cooling systems can lead to significant performance improvements without requiring additional energy inputs, making them a sustainable choice for electric vehicle

manufacturers. Furthermore, the study provides a foundation for future research into optimising VG design and placement, offering invaluable insights for engineers and researchers working beyond electric vehicles, such as renewable energy storage systems. It should be noted, however, that further study, development and testing are required to verify the efficacy, reliability and safety of these proposed enhancements.

Acknowledgment
The authors would like to thank Universiti Teknikal Malaysia Melaka (UTeM), particularly their Faculty of Mechanical Technology and Engineering. This research was not funded by any grant.

References

[1] Shaikh, Ummid Isamiya, Dhanapal Kamble and Sandeep Kore. "A Review on Cooling Methods of Lithium-Ion Battery Pack for Electric Vehicles Applications." *Journal of Advanced Research in Fluid Mechanics and Thermal Sciences* 115, no. 2 (2024): 113-140. https://doi.org/10.37934/arfmts.115.2.113140

[2] Zuber, Mohammad, K. N. Chethan, Laxmikant G. Keni, Irfan Anjum Badruddin Magami and Chandrakant R. Kini. "Enhancing Electric Vehicle Battery Thermal Management using Phase Change Materials: A CFD Analysis for Improved Heat Dissipation." *CFD Letters* 16, no. 8 (2024): 138-149. https://doi.org/10.37934/cfdl.16.8.138149

[3] Napa, Nagaraju, Manish Kumar Agrawal and Bhaskar Tamma. "Design of novel thermal management system for Li-ion battery module using metal matrix based passive cooling method." *Journal of Energy Storage* 73 (2023): 109119. https://doi.org/10.1016/j.est.2023.109119

[4] Behi, Hamidreza, Mohammadreza Behi, Danial Karimi, Joris Jaguemont, Morteza Ghanbarpour, Masud Behnia, Maitane Berecibar and Joeri Van Mierlo. "Heat pipe air-cooled thermal management system for lithium-ion batteries: High power applications." *Applied Thermal Engineering* 183 (2021): 116240. https://doi.org/10.1016/j.applthermaleng.2020.116240

[5] Yang, Xiaowei, Zhiyuan Zhao, Yu Liu, Rong Xing and Yuzhen Sun. "Simulation of nanofluid-cooled lithium-ion battery during charging: A battery connected to a solar cell." *International Journal of Mechanical Sciences* 212 (2021): 106836. https://doi.org/10.1016/j.ijmecsci.2021.106836

[6] Hong, L. B., M. S. Zakaria and H. Abdullah. "Effect of vortex generator on blood flow characteristic on idealized prosthetic heart valve." In *AIP Conference Proceedings*, vol. 2339, no. 1. AIP Publishing, 2021. https://doi.org/10.1063/5.0044170

[7] Salleh, Nursyaira Mohd, Mohamad Shukri Zakaria, Mohd Juzaila Abd Latif and Adi Azriff Basri. "A Computational Study of a Passive Flow Device in a Mechanical Heart Valve for the Anatomic Aorta and the Axisymmetric Aorta." *CFD Letters* 13, no. 4 (2021): 69-79. https://doi.org/10.37934/cfdl.13.4.6979

[8] Hafidzal, M. H. M., W. M. F. W. Mahmood, M. Z. A. Manaf, M. S. Zakaria, M. N. A. Saadun and M. N. A. Nordin. "Soot particle trajectories of a Di diesel engine at 18 ATDC crankshaft angle." In *IOP Conference Series: Materials Science and Engineering*, vol. 50, no. 1, p. 012003. IOP Publishing, 2013. https://doi.org/10.1088/1757-899X/50/1/012003

[9] Basri, Adi Azriff, Muhammad Zuber, Mohamad Shukri Zakaria, Ernnie Illyani Basri, Ahmad Fazli Abdul Aziz, Rosli Mohd Ali, Masaaki Tamagawa and Kamarul Ariffin Ahmad. "The hemodynamic effects of paravalvular leakage using fluid structure interaction; Transcatheter aortic valve implantation patient." *Journal of Medical Imaging and Health Informatics* 6, no. 6 (2016): 1513-1518. https://doi.org/10.1166/jmihi.2016.1840

[10] Zakaria, Mohamad Shukri, Kahar Osman and Haslina Abdullah. "Greenhouse gas reduction by utilization of cold lng boil-off gas." *Procedia Engineering* 53 (2013): 645-649. https://doi.org/10.1016/j.proeng.2013.02.083

[11] Zakaria, Mohamad Shukri, Kahar Osman, Ahmad Anas Yusof, Mohamad Hafidzal Mohd Hanafi, Mohd Noor Asril Saadun and Muhammad Zaidan Abdul Manaf. "Parametric analysis on boil-off gas rate inside liquefied natural gas storage tank." *Journal of Mechanical Engineering and Sciences* 6 (2014): 845-853. https://doi.org/10.15282/jmes.6.2014.10.0080

[12] Li, Xinke, Jiapei Zhao, Jiabin Duan, Satyam Panchal, Jinliang Yuan, Roydon Fraser, Michael Fowler and Ming Chen. "Simulation of cooling plate effect on a battery module with different channel arrangement." *Journal of Energy Storage* 49 (2022): 104113. https://doi.org/10.1016/j.est.2022.104113

[13] Jindal, Prashant, Pranjal Sharma, Manit Kundu, Shubham Singh, Deepak Kumar Shukla, Vikram Jit Pawar, Yang Wei and Philip Breedon. "Computational Fluid Dynamics (CFD) analysis of Graphene Nanoplatelets for the cooling of a multiple tier Li-ion battery pack." *Thermal Science and Engineering Progress* 31 (2022): 101282. https://doi.org/10.1016/j.tsep.2022.101282

[14] Xie, Jinhong, Zijing Ge, Mengyan Zang and Shuangfeng Wang. "Structural optimization of lithium-ion battery pack with forced air cooling system." *Applied Thermal Engineering* 126 (2017): 583-593. https://doi.org/10.1016/j.applthermaleng.2017.07.143

[15] Sparrow, E. M., J. P. Abraham and W. J. Minkowycz. "Flow separation in a diverging conical duct: Effect of Reynolds number and divergence angle." *International Journal of Heat and Mass Transfer* 52, no. 13-14 (2009): 3079-3083. https://doi.org/10.1016/j.ijheatmasstransfer.2009.02.010

[16] Shahid, Seham and Martin Agelin-Chaab. "Analysis of cooling effectiveness and temperature uniformity in a battery pack for cylindrical batteries." *Energies* 10, no. 8 (2017): 1157. https://doi.org/10.3390/en10081157

[17] Mangrulkar, Chidanand K., Ashwinkumar S. Dhoble, Shyamal G. Chakrabarty and Uday S. Wankhede. "Experimental and CFD prediction of heat transfer and friction factor characteristics in cross flow tube bank with integral splitter plate." *International Journal of Heat and Mass Transfer* 104 (2017): 964-978. https://doi.org/10.1016/j.ijheatmasstransfer.2016.09.013

[18] Elmekawy, Ahmed M. Nagib, Alaa A. Ibrahim, Abdalrahman M. Shahin, Sara Al-Ali and Gasser E. Hassan. "Performance enhancement for tube bank staggered configuration heat exchanger–CFD Study." *Chemical Engineering and Processing-Process Intensification* 164 (2021): 108392. https://doi.org/10.1016/j.cep.2021.108392

[19] Celik, Ishmail B., Urmila Ghia, Patrick J. Roache and Christopher J. Freitas. "Procedure for estimation and reporting of uncertainty due to discretization in CFD applications." *Journal of fluids Engineering-Transactions of the ASME* 130, no. 7 (2008). https://doi.org/10.1115/1.2960953